Stability of kangaroo rat burrows in the Sonoran Desert: Evidence of biocementation

Sera Tirkes[1], Duygu Aydin[2], Madison Thompson[3], Clint E. Collins[4], Haluk Beyenal[5], and Idil Deniz Akin[6]*

[1]Graduate Research Assistant, University of California Los Angeles, Department of Civil and Environmental Engineering, Los Angeles, CA 90095, seratirkes@g.ucla.edu
[2]Graduate Research Assistant, School of Chemical Engineering and Bioengineering, Voiland College of Engineering and Architecture, Washington State University, Pullman, WA 99163, duygu.aydin@wsu.edu
[3]Graduate Research Assistant, Sacramento State University, Department of Biological Sciences, Sacramento, CA, madisonthompson2@csus.edu
[4]Assistant Professor, Sacramento State University, Department of Biological Sciences, Sacramento, CA, clint.collins@csus.edu
[5]Professor, School of Chemical Engineering and Bioengineering, Voiland College of Engineering and Architecture, Washington State University, Pullman, WA 99163, beyenal@wsu.edu
[6]*Corresponding author, Associate Professor, University of California Los Angeles, Department of Civil and Environmental Engineering, Los Angeles, CA 90095, idilakin@g.ucla.edu

Abstract
Kangaroo rats (*Dipodomys deserti*) construct complex burrow systems in loose desert sand that survive temperature and relative humidity fluctuations and storms. Animals that burrow in desert sand typically burrow in compacted sand, near plant roots, or when the soil is unsaturated. However, these processes are insufficient to explain tunnel stability of kangaroo rats. Our goal is to understand how kangaroo rat burrows remain stable in loose desert sand, intending to translate this knowledge to geotechnical engineering. A kangaroo rat habitat in the dunes of The Sonoran Desert, AZ, was selected for the study. Dynamic cone penetrometer tests performed at active, abandoned, and no-burrow sites demonstrated that the animals prefer loose sand for burrow construction. Soil samples collected from the burrows' ceilings, subsurface, and surface were characterized. Brazilian tensile strength test results showed that burrow soil has approximately 3 times greater tensile strength than the rest at dry state, which indicates increased interparticle attractive stress in burrow ceilings due to biocementation. Laboratory experiments, scanning electron microscopy, and confocal microscopy images showed that fungal and microbial biofilms provided 17 kPa increase in interparticle attractive stress at less than 1% biomass concentration, indicating potential to be used in soil improvement applications.

Keywords
Kangaroo rat, sand, tensile strength, biofilm, EPS

1. Introduction

Kangaroo rats (Fig. 1a) are keystone desert mammals that are known for their well-developed burrow systems in loose sand where they live and store food (Anderson and Allred 1964; Reichman et al. 1985). They feed on the seeds of desert vegetation. When seeds are available, kangaroo rats collect and carry them in their external cheek pouches and store them in the burrows. Hundreds of thousands of seeds may be found in a burrow (Vorhies and Taylor 1922). Therefore, if a burrow collapsed, kangaroo rats would lose not only their shelter but also their food supply. Perhaps to prevent such a disaster, kangaroo rats carefully construct their burrows. It may take up to two years for kangaroo rats to construct their elaborate burrows (Best 1972). After construction, kangaroo rats occupy the same burrow for an extended period. Young kangaroo rats of some species are known to inherit their burrows from their parents (Jones 1984). During this time, kangaroo rats actively maintain the stability of their burrows, which may collapse after the animals abandon them (Hawkins and Nicoletto 1992). The burrows survive severe temperature and relative humidity (RH) fluctuations on both a yearly and daily basis, and possibly withstand multiple convective rainfall events or high-intensity storms throughout years (Kay and Whitford 1978; Burda et al. 2007).

Tunneling in loose sand without permanent support is a challenge for geotechnical engineers (Takano 2000; BTC 2004). However, some desert mammals are able to build complex, perennial burrow systems that last decades using fundamental soil mechanics principles. The stability of burrows in desert sand can be explained by unsaturated soil mechanics, compaction, and bio-reinforcement (Kinlaw 1999; Akin et al. 2023). For example, Damara mole-rats *(Cryptomys damarensis)* build their burrows only if the soil is unsaturated after a flood event when capillary interparticle stresses are maximum (Lovegrove and Painting 1987). Round-tailed ground squirrels

(Spermophilus tereticaudus) perform a violent shaking motion during their excavation process potentially to compact the soil after digging the burrows (Drabek, 1970). Many animals dig their tunnels near plant roots of shrubs to take advantage of bio-reinforcement, thus tunnels are physically supported by the roots (Kinlaw 1999). However, no evidence indicates kangaroo rats (*Dipodomys deserti*) exploit elevated attractive capillary interparticle stresses by constructing only after a rain event, compacting during construction, or constructing only near the plant roots (Akin et al. 2023). Understanding how kangaroo rat burrows solve a geotechnical challenge could provide new bioinspired geotechnical solutions. Therefore, the goal of this study is to understand how kangaroo rat burrows stay stable in loose sand.

A study site consisting of sand dunes containing active and abandoned burrows located several meters from the nearest plants in the Sonoran Desert, near Yuma, AZ was selected. Dynamic cone penetrometer tests were conducted to determine if soil density near animal burrows is different from no-burrow sites and to understand the influence of soil compaction on the animals' site selection preference. Bulk soil samples were collected from the ceilings of the abandoned burrows, from the desert surface, and from the subsurface (0.5 m) to quantify the attractive interparticle stresses in the laboratory using a small-scale Brazilian tensile strength (BTS) test. A limit-equilibrium tunnel stability analysis was conducted to quantify the minimum required attractive interparticle stress to maintain the stability of the burrows and the results were compared with the BTS results. Scanning electron microscopy and confocal laser scanning microscopy with specific staining were used to evaluate the microstructure of the burrow soil and biological substances that provide an increased interparticle attractive stress to burrow soil through biocementation.

2. Materials and Methods

2.1. Study Site and Sample Collection

The study site was selected in *D. deserti* habitat in the sand dunes of the Sonoran Desert, near Yuma AZ (Fig. 1). This part of the Sonoran Desert is also known as the Yuma Desert and consists of low sandy plains, extensive dunes, and scattered hills of highly eroded volcanic rock (Jaeger 1957). The area has minimal precipitation and high daily and seasonal temperature fluctuations. For example, in 2022 the area received 1 mm/year of precipitation in the form of high-intensity, short-duration rainstorms, and summer temperatures reached 45 °C while winter temperatures fell below 3 °C in the same year (NOAA 2022). Field testing and sampling was performed away from any plants.

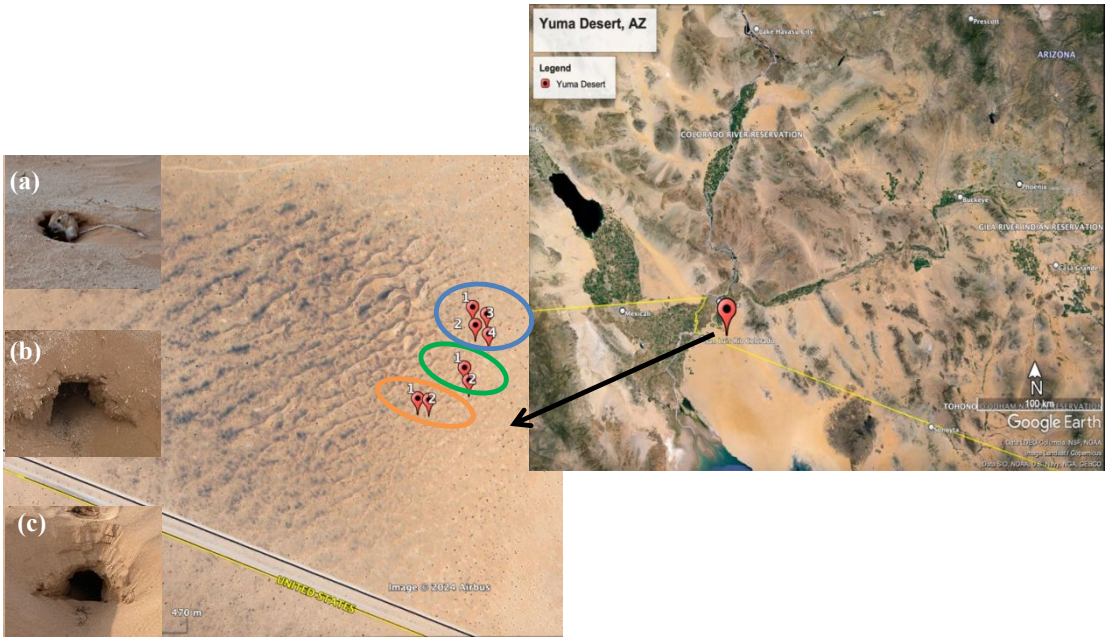

Fig. 1. Map of the Study Site, (Google Earth, Yuma Desert, AZ, 2023). (a) Desert Kangaroo Rat, *Dipodomys deserti* habitat including (b) abandoned burrows and (c) active burrows. Bulk soil sample collection locations: burrow sand (blue), subsurface sand (orange), and surface sand (green)

The kangaroo rat burrows were distributed over a large area. Active and abandoned burrows were present at the site, with the total burrow area extending beyond a 3.3 km perimeter and 78.5 hectares. The site was divided into three subsections for sampling and field testing: active burrow sites, abandoned burrow sites, and no-burrow sites. The division was made based on field observations. Activity around entrances including recent kangaroo rat spoor, which were wind-swept clean each day, were used to distinguish between active and abandoned burrows (Fig.1). Active burrows were identified if kangaroo rat footprints, tail drag, and fresh sand excavated from the tunnel spread around the entrance like an apron were observed near the entrances. In addition, a round tunnel ceiling and a well-kept floor were characteristics of active burrows. Irregular tunnel shape, spider webs, and straws at or inside the tunnel entrances indicated abandoned burrows. The no-burrow site was selected if no burrow openings were visible within the vicinity of a location. This was 8.4 m away from the nearest active burrow site in the field. The geometry of active burrows was used to perform tunnel stability analysis; however, burrow ceiling samples were collected from the abandoned burrows not to disturb the kangaroo rat habitat.

Bulk soil was collected from each site in three 5-gallon buckets. At the abandoned burrow site, soil samples were collected from the ceilings of the abandoned burrows using hand shovels and spatulas. These samples will be referred as “burrow sand.” At the active burrow site, soil samples were collected from approximately 50 cm deep trenches near the active burrow entrances. The samples collected at this location reflect subsurface desert soil and will be referred to as “subsurface sand.” Soil samples at the no-burrow site were collected from the top 10 cm depth using shovels to reflect the surficial desert sands and will be referred as “surface sand.”

In addition to bulk sand samples, burrow sand was sampled from the ceilings of abandoned burrows using sterilized spatulas for microscopy imaging. Approximately 1 mL of sand was placed

on sterile malt extract agar (MEA) plates and tryptic soy agar (TSA) plates. The selected media facilitates the growth of fungi or bacteria. MEA only facilitates the growth of fungi at pH 3.5 and TSA only facilitates the growth of bacteria. The purpose of enriching microbes on agar plates is to scale up biocementation processes for a clear visualization of the impact of bacterial and fungal biofilms on the sand matrix. The plates were prepared beforehand in the laboratory. TSA plates were prepared by suspending 40 g tryptic soy agar (BD Difco™, cat. no. DF0369-17-6) in 1 L distilled water and autoclaving at 121 ^{o}C for 15 min. MEA plates were prepared by suspending 50 g malt extract agar (Sigma Aldrich, cat. no. 70145) in 1 L distilled water and autoclaving at 121 ^{o}C for 15 min. For the inhibition of bacterial growth, 2 mL of 10% sterile lactic acid (Sigma Aldrich, cat. no. 69785) was added to the MEA medium to adjust the pH to 3.5. The samples and the agar plates were preserved in a water-tight container and cold-stored on ice until they were transported back to the laboratory. The sand-filled agar plates were preserved at 4 ^{o}C to slow down microbial and fungal activity before microscopy imaging.

2.2. Burrow Network Geometry

A tunnel of a recently abandoned burrow far from the DCP locations was excavated to determine the geometry of the burrow network in the field after the part of the tunnel was partially collapsed during measurement. Plaster of Paris (6 kg) was mixed with water (3 kg). The mixture was stirred to get the proper consistency to pour inside the burrow. The burrow was completely filled with the plaster and excavated after 24 h with hand shovels avoiding damage to the hardened plaster. The measurements of the burrow were noted as length, depth, and diameter of the tunnels; entrance slopes; entrance slopes of the side tunnels.

2.3. Soil Characterization

The particle size distribution curve was measured with dry and wet sieve analysis according to ASTM D6913 and ASTM D1140. Specific gravity was measured according to ASTM D854, and minimum-maximum void ratios tests were determined according to ASTM D4245. Additionally, a loss-on-ignition (LOI) test was conducted when quantifying polymer content as described by Scalia IV et al. 2014 to find the organic matter content of the desert soil. Samples were placed in a 550 ^{o}C furnace for 4 h. All characterization tests were repeated at least 3 times while both the average and the standard deviation were recorded (Table 1).

Table 1. Soil properties. G_s: Specific gravity, $e_{min,\ max}$: minimum, maximum void ratio, d_{50}: mean particle size diameter (mm), c_u: coefficient of uniformity, c_c: coefficient of curvature and fines percent (%), *LOI*: Loss-on-ignition (%).

Property	Burrow Sand	Subsurface Sand	Surface Sand
G_s	2.64 ± 0.003	2.64 ± 0.014	2.67 ± 0.016
e_{max}	0.82 ± 0.002	0.88 ± 0.012	0.89 ± 0.013
e_{min}	0.56 ± 0.006	0.61 ± 0.020	0.60 ± 0.006
d_{50}	0.12	0.12	0.16
C_u	2.00	1.67	1.80
C_c	0.95	0.82	0.80
Fines	7.97	2.95	2.31
LOI	0.94	1.11	0.79

Mineral composition of the soils collected from each of the three sites were determined with X-ray diffraction (XRD) analysis. PANalytical Empyrean XRD was run with a Cu X-ray tube, 2.3° divergence soller slits, 5-, 10-, and 15-mm mask, and a PIXcel-1D detector. The XRD spectrums were collected at a wavelength of 1.54 Å, at room temperature (25 ^{o}C), over 2θ range of 10° to 90°, with a step size of 0.026°. Diffraction patterns were analyzed with HighScore Plus software to identify phases.

Exchange complex (Table 2) of the soils was determined by Best Test Laboratories (Moses Lake, WA) using the sodium acetate method. Soil samples (2.0 g ± 0.1 g) were first rinsed with 1N sodium acetate solution, followed by a 99.8% methanol rinse, and a 1N ammonium acetate rinse. The amount of sodium in the extract was measured after the ammonium acetate rinse with a spectrophotometer (Horneck et al. 1989). The bound cations were predominantly Ca^{2+}. The difference between the exchange complex of burrow, subsurface, and surface soil was not statistically significant.

Table 2. Exchange complex of burrow, subsurface and surface sand.

Bound Cations (%)	Burrow	Subsurface	Surface
Ca^{2+}	73	76	63
Mg^{2+}	11	14	15
K^{+}	6.9	9.7	13
Na^{+}	0.4	1.4	0.7
CEC (meq/100g)	*4.5*	*3.7*	*2.7*

2.4. Smart Dynamic Cone Penetrometer (DCP) Test

Dynamic Cone Penetrometer (DCP) tests were conducted in each subsection (Fig. 1) using a Smart DCP (VERTEK, Randolph, VT) as described in ASTM D6951. The 60° cone of the DCP with a 20 mm base diameter was driven into the soil by dropping a 4.6 kg hammer from 57.5 cm height. The total penetration for a given number of blows was measured with a laser and automatically recorded in mm/blow using a smartphone. DCP has been commonly used on sandy soil profiles (Gomez et al. 2015; Ghasemi and Montoya 2022) and selected for this study because of its relatively easy setup in the desert environment and high measurement accuracy.

The relationship between the number of blows and depth of penetration at a given linear depth segment was recorded as the DCP penetration index, *DPI* (Embacher 2006). Using the *DPI*, the relative density D_r (%) of the soil profile was calculated according to eq. 1 (Mohammadi et al. 2008), which was derived based on a series of laboratory tests at constant void ratios.

(1) $$D_r(\%) = \frac{189.93}{(DPI)^{0.53}}$$

Based on eqn. 1, the soil layers were classified as very loose (*DPI* > 42 mm/blow and D_r < 25 %), loose (*DPI* = 42 to 23 mm/blow and D_r = 25 to 35 %), medium (*DPI* = 23 to 12 mm/blow and D_r = 35 to 50 %), dense (*DPI* = 12 to 5 mm/blow and D_r = 50 to 75 %), or very dense (*DPI* < 5 mm/blow and D_r > 75 %).

2.5. Tunnel Stability Analysis

The stability of the burrows was analyzed using the upper limit theorems of plasticity. The work rate calculation for the upper bound that defines an unsafe stress level involves the self-weight of the soil and the corresponding tunnel pressure based on kinematic collapse mechanisms (Atkinson and Potts 1977; Davis et al. 1980). Burrow stability analysis was performed according to Espinoza and Santamarina (2010) equivalent continuum limit analysis (eq. 2)

(2) $$A = W\ x\ (\frac{6}{\alpha\pi}(1-n)\frac{D}{d_{50}})$$

where *A* is the minimum net attractive interparticle force required for tunnel stability, *W* is the self-weight of the soil grains, α is the geometric parameter (1 for 2D and 2 for 3D analysis), *D* is the tunnel diameter, d_{50} is the average grain size, and *n* is the porosity. The geometric parameter was taken as 1 in this study.

For an uncemented unsaturated sand, the maximum theoretical attractive interparticle stress due to capillary and van der Waals forces were calculated according to simple cubic (SC) and tetrahedral (TH) packing of sand particles, where the force is spread over the unit cell area, $4R^2$

(for SC) and $8R^2$ (for TH) with R being the grain size radius. The capillary force, F_{cap}, is defined as Santamarina et al. (2001):

$$(3) \quad F_{cap} = \frac{\pi}{2} T_s d_{50} \left[2 - \left(\frac{8}{9} w G_s \right)^{\frac{1}{4}} \right]$$

where w is gravimetric water content (up to 0.06), T_s is air-water surface tension (0.072 N/m at 25 ^{o}C), d_{50} is the mean grain size diameter, G_s is the specific gravity. Sand particles were assumed to be monosized spheres.

The van der Waals force, F_{vdw}, was calculated according to eq. 5 (Santamarina and Fam 1995; Santamarina et al. 2001; Israelachvili 2011) as:

$$(4) \quad F_{vdw} = \frac{A_h}{24 t^2} d_{50}$$

where A_h is the Hamaker constant (6.5 x 10^{-20} J at dry condition and 6.4 x 10^{-21} J at saturated condition) and t is the particle separation distance that was taken as 2 nm.

2.6. Brazilian Tensile Strength (BTS) Test and Suction Stress

BTS tests were conducted as described in (Akin and Likos 2017a). Disk-shaped specimens with 3 cm diameter and 1 cm thickness were prepared using a custom-made compaction mold (Akin and Likos 2017a). Bulk soil samples were recompacted into disk-shaped specimens as undisturbed samples could not be obtained in the field. Bulk soil (14.2 g) at 10% water content was compacted in the mold to 0.46 ± 0.02 void ratio. Ten specimens were prepared with each soil sample (i.e., burrow sand, subsurface sand, and surface sand). After compaction, specimens were dried following three methods: air dry, 105 °C oven-dry, and 40 °C oven-dry. Specimens were placed between two curved bearing blocks having a 14° arc of contact with the specimen and compressed using a 35 kPa capacity load cell with a constant displacement rate of 0.3 mm/min until the specimens broke along the vertical diameter. All specimens failed within 3 min. The

gravimetric water content of the specimens measured post-test verified that all three drying methods resulted in fully-dry specimens and indicated that water uptake during the BTS test was less than 0.40% for air-dry, 0.30% for 40 °C oven-dry, and 0.15% for 105 °C oven-dry specimens.

Tensile strength, $\sigma_{t,}$ was calculated according to (Hondros 1959):

(5) $$\sigma_t = -\frac{2P}{\pi dt}$$

where P is the compressive force at failure, d is the specimen diameter, and t is the specimen thickness.

The suction stress was quantified using the tensile strength as described in (Akin and Likos 2017b):

(6) $$p = \frac{1}{3}(\sigma_x + \sigma_y + \sigma_z)$$

(7) $$q = \frac{1}{\sqrt{2}}\sqrt{(\sigma_y - \sigma_z)^2 + (\sigma_y - \sigma_x)^2 + (\sigma_z - \sigma_x)^2}$$

(8) $$p' = p - \sigma^s$$

where σ^s is the suction stress (or the resultant attractive stress), p is the mean total stress, p' is the mean effective stress, q is the deviatoric stress, $\sigma_x = \sigma_t$ with corresponding orthogonal stresses $\sigma_y = -3\sigma_x$ and $\sigma_z = 0$. A linear failure envelope was plotted using internal friction angle ϕ in p'- q space with slope m where $m = (6\sin\phi)/(3 - \sin\phi)$. A critical state friction angle of 31° was used for the analysis. The difference in mean stress between the total stress envelope ($p - q$) and the effective stress envelope ($p' - q$) is reported as the resultant attractive stress (σ^s).

2.7. Microscopy Imaging

Two sets of scanning electron microscopy (SEM) images were taken with burrow sand to evaluate the presence of cementation between sand particles. In the first set, SEM images of the in-situ sand samples were taken with Variable Pressure Scanning Electron Microscope (VPSEM)–Hitachi SU3900 or FEI Verios 460L (FEI-SEM). The VPSEM is equipped with a standard

Everhard-Thornley secondary electron detector and a five-segment solid state backscattered electron detector. Samples imaged with VPSEM were coated with 1 nm gold and palladium to observe roundness and angularity of the sand grains. FEI-SEM is an ultra-high resolution Schottkey emitter SEM and was used to resolve presence of cementation between sand grains due to better resolutions at higher magnifications. For this microscope, the soil samples were coated with 3 nm gold and palladium.

In the second set, the burrow sand samples on MEA and TSA plates were incubated to induce microbial and fungal growth and scale up the bio-cementation. Burrow sand samples were fixed to preserve the structure of microbes. The fixation process was done by adding 2% paraformaldehyde (Electron Microscopy Sciences, cat. no. 15710), 2% glutaraldehyde (Electron Microscopy Sciences, cat. no. 16320), and 0.1 M sodium phosphate buffer. The sodium phosphate buffer (pH 7.2) was prepared by mixing 17.85 g sodium phosphate dibasic heptahydrate (J. T. Baker™, cat. no. 02-004-206) and 1.41 g sodium phosphate monobasic monohydrate (J. T. Baker™ cat. no. 02-004-202) in 1 L of deionized water (DI). The samples were incubated overnight at 4 ^{o}C and washed with 0.1 M sodium phosphate buffer three times in 10 min intervals. The samples were dehydrated through a series of 30%, 50%, 70%, 90%, and 100% ethanol solutions. Finally, 100% hexamethyldisilazane (HMDS) solution (Electron Microscopy Sciences, cat. no. 16700) was added and left overnight for final drying. The fixed samples were then mounted on stubs, gold coated, and imaged with SEM (Quanta 200F, Hillsboro, OR).

Additionally, confocal scanning laser microscope (CSLM, (TCS SP-8, Leica Microsystems, Buffalo Grove, Il)) was used to verify the presence of biofilm formation and extracellular polymeric substances (EPS) within the matrix in the burrow sand samples enriched on MEA and

TSA plates. For the evaluation of live and dead microbes and fungi, samples were stained with 300 nM DAPI (4′,6-diamidino-2-phenylindole) live/dead stain (Thermo Fisher Scientific, D1306) and washed 3 times with 0.1 M Phosphate-buffered saline (PBS) at pH 7.4 after 5 min of incubation (Glöckner et al. 1999). The imaging was performed with 430 nm to 500 nm emission band. To verify the presence of lipid molecules, samples were prepared as described in (Ostle and Holt 1982). The slides were heat fixed, stained with 1% Nile Blue-A solution (Thermo Fisher Scientific, 415690100), and incubated at 55 °C for 10 min. The slides were then washed with 8% acetic acid for 1 min and the excess dye was washed with water (Ostle and Holt, 1982). The prepared samples were examined with 600 to 700 nm emission wavelength range (Gattuso *et al.*, 2016). For the identification of the biofilm matrix, samples were heat fixed and stained with FilmTracer™ SYPRO® Ruby biofilm matrix stain (Thermo Fisher Scientific, F10318). 200 µL FilmTracer™ SYPRO® Ruby biofilm matrix stain was added to the burrow sand samples and incubated at room temperature (25 °C) for 30 min, protected from light. After the incubation, the excess stain was removed with DI water (Park et al. 2021). The wavelength emission range was chosen as 575 to 710 nm to image the stained samples as indicated in (Loza-Correa et al. 2019).

3. Results and Discussion

3.1. Soil Characterization

The surface and subsurface sand were characterized as poorly-graded sand (SP) according to Unified Soil Classification System (USCS, (ASTM D2487)), whereas the burrow sand was classified as SP-SM (Fig. 2 and Table 1). The angularity of the sands was classified according to Youd (1973) and Powers (1953) as subrounded for the subsurface (C_u = 1.67, C_c = 0.82) and surface sand (c_u = 1.80, c_c = 0.80), and a mixture of subrounded and subangular for the burrow

sand (c_u = 2.00, c_c = 0.95). The burrow sand had 8% fines while the surface and subsurface sand had less than 3% fines.

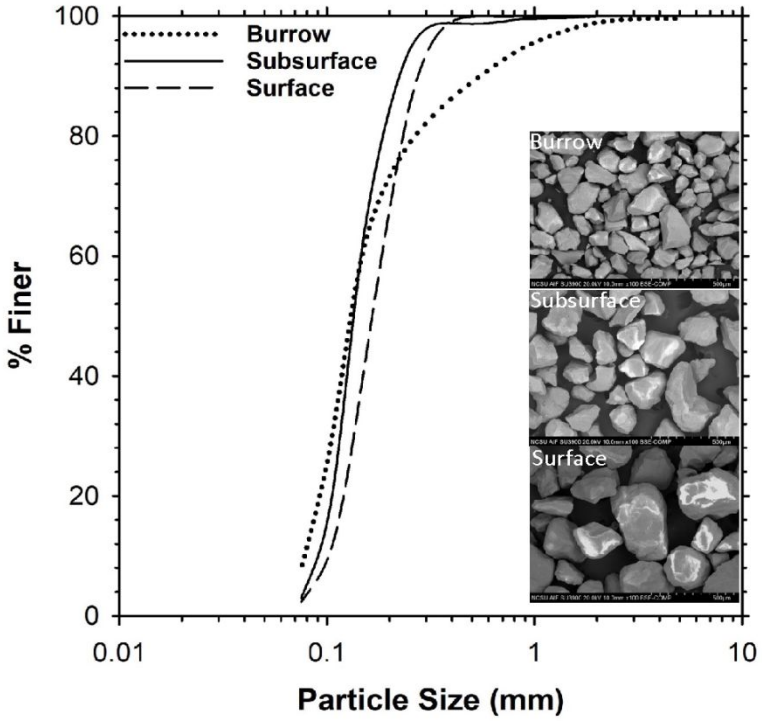

Fig. 2. Grain size distribution curve of burrow sand, subsurface sand, and surface sand in scale of 500 μm VPSEM images.

The mineral composition of the fines was determined with XRD analysis (Fig. 3). The peaks were identified as quartz and feldspars. The feldspars were consisted of albite, plagioclase, and anorthite. In Figure 3, black dashed lines show quartz peaks, red dashed lines show albite and plagioclase, and blue dashed lines show anorthite peaks. The peaks appeared mainly at locations for quartz (Heaney and Post 1992). The peaks were observed at the same positions for both the coarse and fine portion of the sands, suggesting the fines are generated largely because of sand particle erosion. Therefore, unlike silt and clay, the fines in the burrow soil are expected to provide negligible interparticle attractive stress due to van der Waals forces (Akin and Likos 2020).

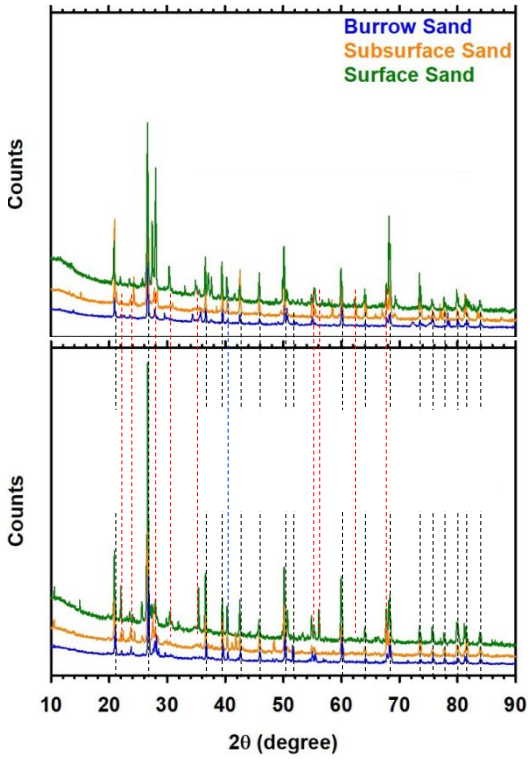

Fig. 3. XRD patterns of (a) unprocessed sand and (b) the fine fraction of sand from the burrows, subsurface, and surface. Black dashed lines show quartz peaks, red dashed lines show albite and plagioclase peaks, and blue dashed lines show anorthite peaks.

3.2. Soil Profile and Kangaroo Rat Burrows

The soil profile generally consisted of a very loose layer (*DPI* > 42 mm/blow) at the top 8 to 20 cm depth (Fig. 4). A *DPI* value of less than 42 mm/blow corresponds to a relative density (D_r) of less than 25%, which is classified as "very loose" (Mohammadi et al. 2008). Such loose surficial layers are commonly deposited in sand dunes by wind. However, three locations (active burrow location 1, no-burrow location 2, and abandoned burrow location 2) had stiffer surface layers that showed low *DPI* values (*DPI* < 9). These stiffer surficial layers were attributed to the presence of desert biocrust (Belnap et al. 2001). Biocrust is commonly seen on desert surfaces and is formed by fungi, cyanobacteria, eukaryotic algae, lichen, and bryophytes (Pietrasiak et al. 2013).

Soil stiffness gradually increased with depth after the surface layer, with few exceptions that showed excessive penetrations, where one blow resulted in an excessive (150 to 200 mm) penetration. The excessive penetrations were attributed to the presence of burrows and are marked on Fig. 4 with arrows. In other words, a kangaroo rat burrow tunnel was discovered during testing far from any burrow entrances. *DPI* was measured in between 150 and 840 mm/blow for all burrows, which corresponds to D_r less than 25%, indicating that kangaroo rats prefer loose soil to construct their burrows. This was attributed to increased digging rate efficiency in loose soil (Sichilima et al. 2008) or increased microbial cementation in loose soil due to availability of pore space (Rodriguez-Navarro et al. 2003; Chou et al. 2011). The results showed that deep burrow complexes were extensive throughout the study site and were hidden from beneath the surface.

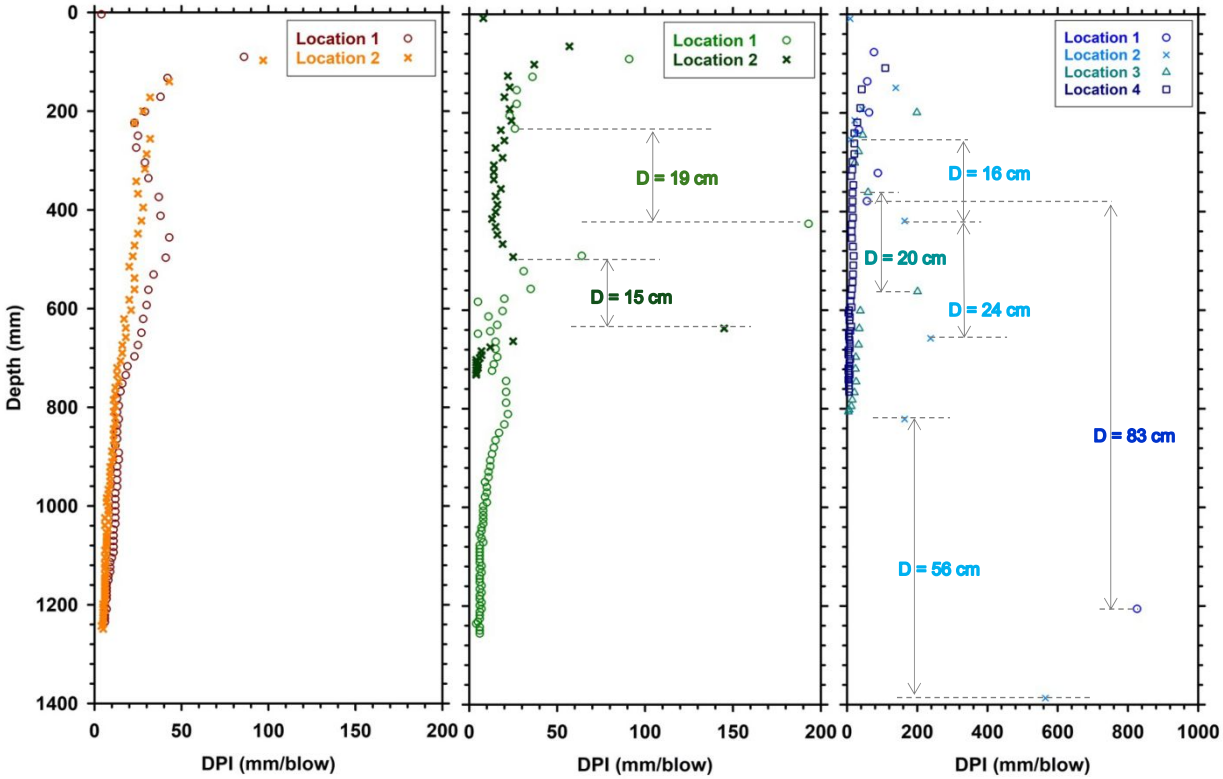

Fig. 4. (a)Active burrow, (b) no-burrow, and (c) abandoned burrow site soil profiles obtained with in-situ smart DCP testing. The burrow locations are indicated with opening sizes and arrows.

The burrow diameters were determined from the DCP data as the depth over which an excessive penetration occurred. Burrow diameters ranged between 15 cm and 83 cm, which is greater than the reported values in the literature that averaged 12 cm (Vorhies and Taylor 1922). The larger-than-expected tunnel diameter may reflect the layered burrow structure with the presence of two tunnels located on top of each other or a different section of the burrow other than the tunnel. Kangaroo rat burrows are complex systems that include different sections with varying diameters including plugs (deeper regions to escape predators) and nest chambers (Vorhies and Taylor 1922; Anderson and Allred 1964) as also shown in the excavated burrow in Fig. 5.

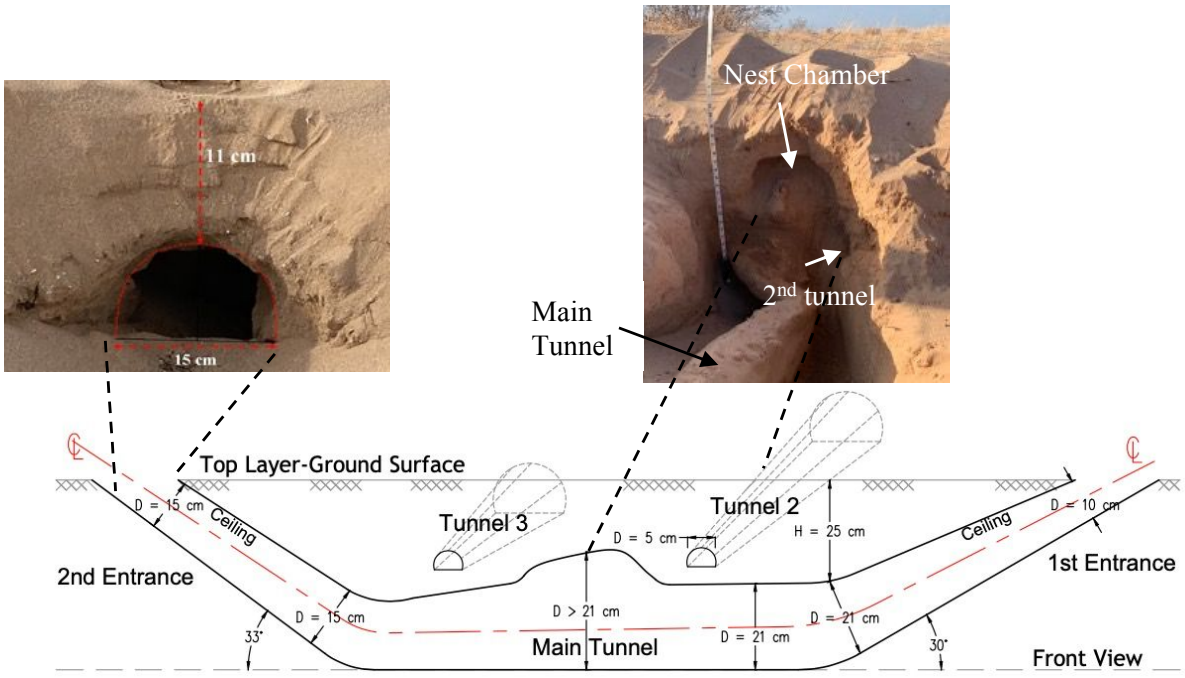

Fig. 5. Cross section of the excavated burrow.

The excavated burrow had two entrances. The first entrance had an arched ceiling, a bottom width of 21 cm and a height of approximately 10 cm. The second entrance had a circular opening with a diameter of 15 cm. Both entrances led to steep tunnels with a slope of 30° or 33° angles. The tunnel connected to the first entrance was 80 cm long and 25 cm deep. The tunnel had a left

turn at 25 cm and connected to the main tunnel. The main tunnel was at approximately 50 cm depth and connected to another tunnel 120 cm away from the entrance. This second tunnel closer to the surface relative to the main tunnel was approximately in 5 cm diameter and inclined at 30°. After the second tunnel, a round, nest-like structure was observed with a diameter higher than 21 cm. Then, a third tunnel was found inclined at 50°. The tunnels collapsed after measuring tunnel three incline. Thus, more measurements could not be taken. The total length between the first and second entrances was 2.6 m.

3.3. Tensile Strength

Tensile strength of the burrow sand was up to 3 times higher than the subsurface sand and 2.5 times higher than the surface sand for all drying conditions (Fig. 6). While the tensile strength of the burrow sand and the surface sand was not affected by drying at 40 °C, drying at 105 °C decreased tensile strength (24% for burrow sand, 14% for subsurface sand, and 20% for surface sand). The reduction was attributed to the decrement of biological substances because the binding substances produced by organisms such as fungi may begin to ablate when the temperature exceeds 50 °C (Mataix-Solera et al. 2011).

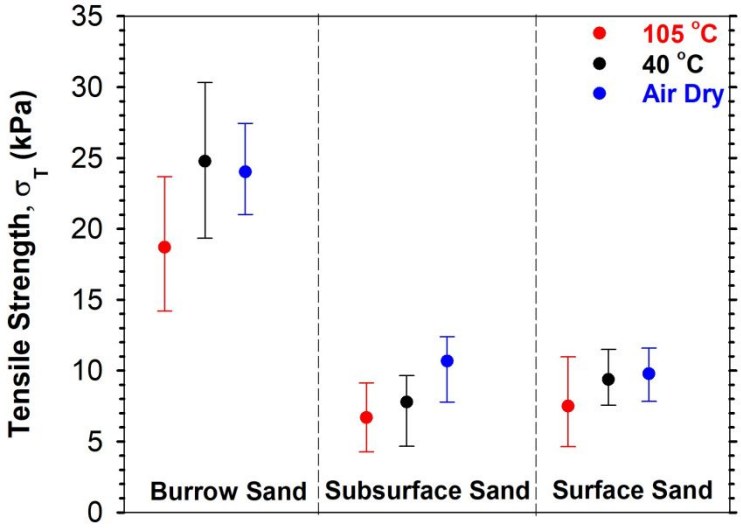

Fig. 6. Brazilian tensile strength (BTS) at dry condition for burrow sand, subsurface sand, and surface sand.

3.4. Burrow Stability Analysis

The limit attractive interparticle stress needed for tunnel stability is shown for each tunnel diameter for SC and TH packing (Fig. 7, symbols). The lines show the limits for stability for SC and TH conditions, where the area below each line represents unstable conditions. Given attractive physiochemical and capillary stresses, the minimum required attractive stress for tunnel stability for the smallest diameter tunnel was 2.0 kPa for SC (D_r < 25%) and 5.8 kPa for TH (D_r > 75%) packing and that for the largest diameter tunnel was 11.3 kPa for SC and 32.1 kPa for TH packing (Fig. 7).

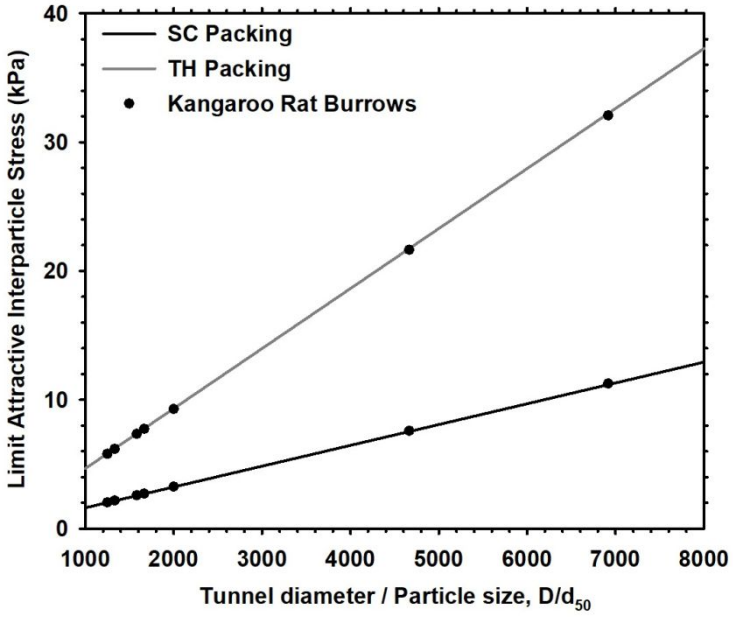

Fig. 7. Relationship between tunnel diameter to particle diameter ratio and required attractive interparticle stress considered for simple cubic (SC) and tetrahedral (TH) packing conditions to prevent kangaroo rat burrows to collapse.

The limit attractive interparticle stress, calculated from the net attractive interparticle force (A), is equivalent to suction stress. This stress comprises capillary attraction and physicochemical attraction, which results from van der Waals attraction and double-layer repulsion (Lu and Likos, 2006), as well as cementation. All these factors are independent functions of the degree of

saturation (Akin and Likos 2020; Shariq et al. 2021). For uncemented clean sand, suction stress is primarily influenced by capillarity. However, the presence of surface-active fines introduces physicochemical attraction, mainly due to van der Waals forces under dry conditions (Israelachvili 2011; Akin and Likos 2020). XRD analysis revealed that the fine content of the sand used in this study is predominantly quartz. Therefore, van der Waals attraction and double-layer repulsion were considered negligible for this analysis (Lu and Likos 2006; Akin and Likos 2020). In dry conditions, capillary stress is also zero due to the absence of a water meniscus. Thus, a nonzero value of A in dry conditions indicates cementation, with a minimum of 2.0 kPa attractive stress for the smallest diameter burrow (if the in-situ packing is SC) and a maximum of 32.1 kPa attractive stress for the largest diameter burrow (if the in-situ packing is TH). Laboratory BTS tests under dry conditions confirmed that the burrow sand is cemented, providing a resultant attractive stress of 17 kPa at a void ratio of 0.46.

The upper limit stress from dry sand only considers dilatancy, which includes interlocking and jamming (Cates et al. 1998; Schofield 2006). Although the jamming effect might provide stability in the field to the burrows, its effect for uncemented dry sand is limited to when the tunnel diameter to grain particle size ratio (D / d_{50}) is less than 5.2 (Valdes and Santamarina 2006; Guo and Zhou 2013). In this study, the minimum D / d_{50} was 1250, which is remarkably larger than 5.2. Therefore, the continuum analysis was preferred, which eliminates the jamming effect. In laboratory testing, recompaction lead to consideration of only interparticle attractive stresses for the sand specimens.

3.5. Potential Source of Cementation in The Burrow Sand

Cementing bonds were achieved in the laboratory by activating the native and non-inoculated microbial and fungal biofilms with water and subsequently observed using FEI-SEM. Figures 8a-

8d show bonds between sand grains that likely originate from both fungal and microbial biofilms. To distinguish in between sources of biofilm, scaled up cementation images were obtained with TSA and MEA media.

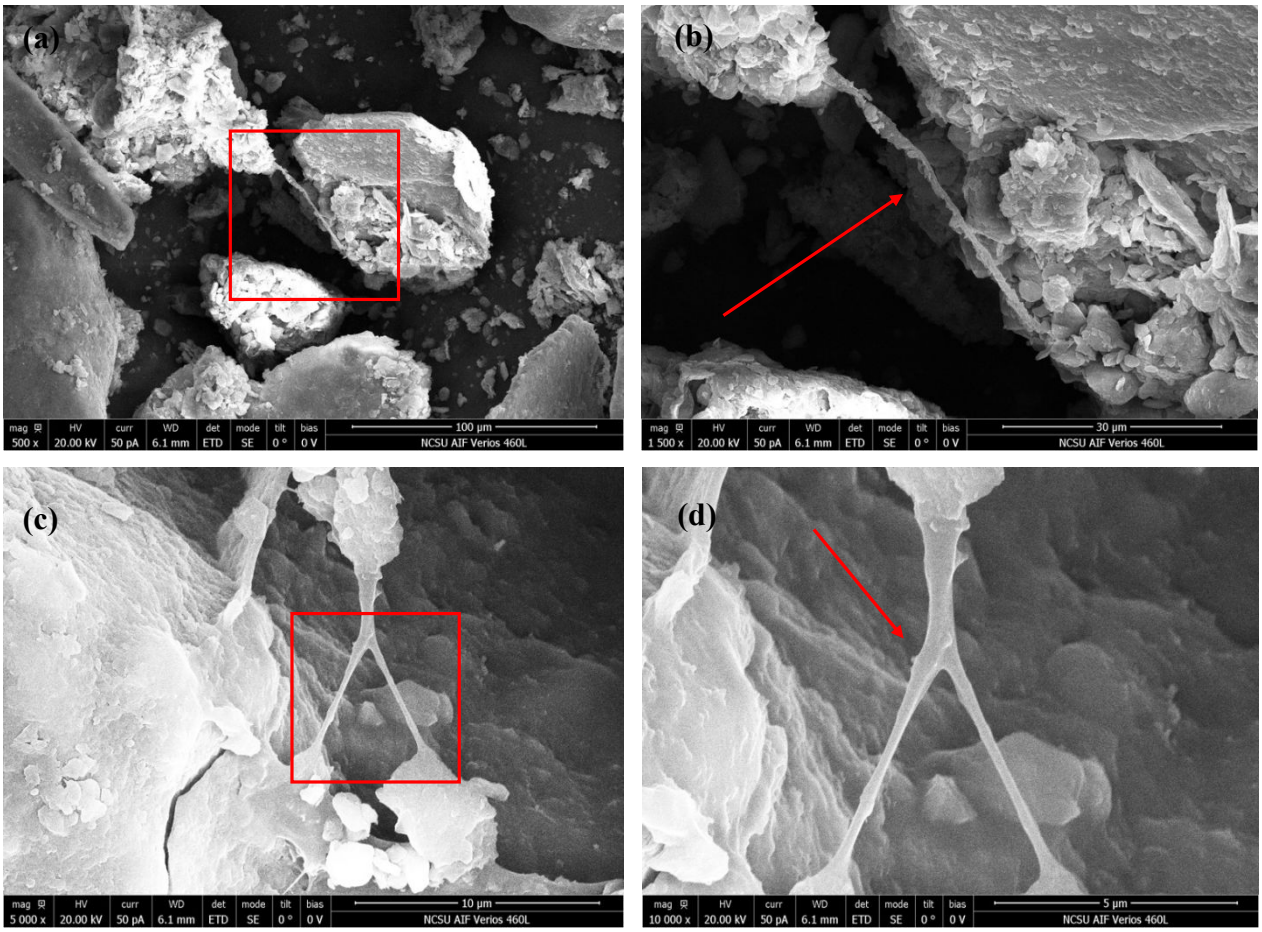

Fig. 8. FEI-SEM images of in-situ burrow sand in scale 100 μm (a), 30 μm (b), 10 μm (c), and 5 μm (d). The focused regions on the sample are shown with rectangles on the images. The fungal hyphae formations are shown with arrows.

The SEM images of scaled up cementation bonds presented in Fig. 9 show evidence of fungal and bacterial biofilms within the burrow sand samples seperately. Figures 9a and 9b highlight the bridging of biofilm formed between two individual sand particles, and Figs. 9c and 9d show the fungal hyphae adhering onto the sand surface and accumulating over multiple particles. This study hypothesized that the source of cementation in the burrow soil was from the activity of microbial

and fungal communities growing as biofilms because biofilms can grow in unfavorable conditions (Lewandowski and Beyenal 2013). Many groups of organisms such as bacteria, yeasts, algae, and filamentous fungi are capable of forming biofilms in soil (Wingender et al. 1999). With the secretion of these molecules and biofilm formation, the cells and sand particles are connected in a matrix holding the sand particles together. The EPS within the matrix promotes aggregation and attachment, cell to cell communication, gene exchange as well as physical structural stability (Decho 2000; Decho and Gutierrez 2017). The biofilm formation also protects microbial communities against unfavorable conditions as it provides nutrients to the cells, retains water, and forms a protective barrier against UV radiation and extreme temperatures (Lewandowski and Beyenal 2013; de Carvalho 2017). Additionally, filamentous fungi have a greater tendency to grow as biofilms as they secrete substantial amounts of EPS in unsaturated environments (Jones 1994; Holden 2001). Fungal biofilms grow from the basic unit structures of filamentous fungi called hyphae. These structures attach and expand invasively across a surface while secreting polymeric substances. The biofilm becomes more complex and reaches its maturity as hyphae propagate to form a large network called mycelium (Peberdy and Peberdy 1980; Harding et al. 2009). The entanglement of individual grains could potentially promote sand aggregation and can be the source of bio-cementation. Such observations have been made in previous literature. For example, Tisdall and Oades (1982) and Chenu (1989) have reported that fungal species contribute to soil stability not only through their morphological properties, such as hyphal formation, but also through EPS secretion capabilities (Tisdall and Oades 1982). Tisdall and Oades (1979) employed SEM to illustrate how EPS connects sand particles together, playing a significant role in bio-cementation.

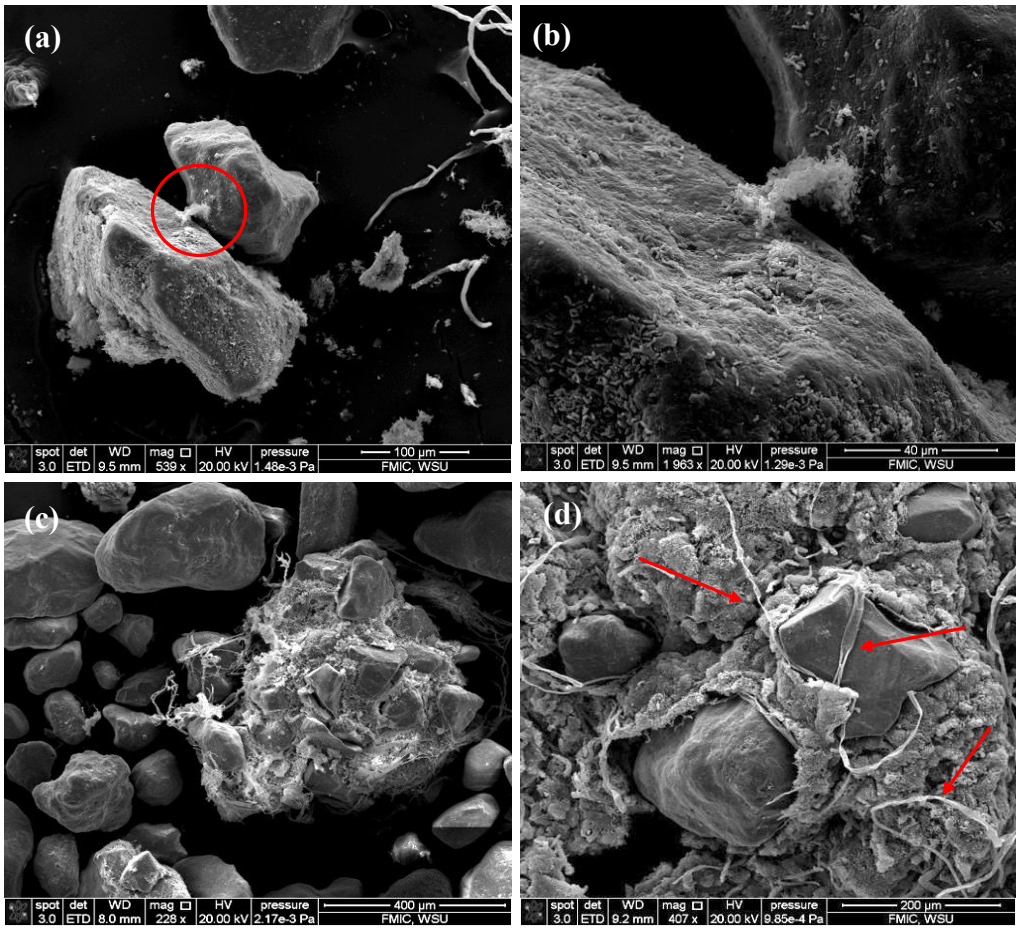

Fig. 9. SEM images of burrow sand samples enriched with TSA in scale (a) 100 µm and (b) 40 µm. The images of enriched with MEA in scale (c) 400 µm and (d) 200 µm. Biofilm is indicated in a circle between two sand particles and the fungal hyphae formations are shown with arrows.

CLSM images with specific staining further demonstrated the presence of biofilm and EPS in the burrow sand samples. Figure 10a shows the CLSM images of burrow sand samples stained with DAPI. These images exhibit the thick layer of cells and the existing eDNA in the matrix in between the individual sand particles. eDNA is an important component of the biofilm matrix as it can promote biofilm formation. For example, *Aspergillus fumigatus*, a common filamentous fungi found in soil and known to have biofilm forming capabilities, excretes eDNA during autolysis when faced with external stress (Rajendran et al. 2013; Fraaije et al. 2020). Figure 10b shows the enriched burrow sand stained with Nile Blue A. Nile Blue A stain highlights the existing

lipid molecules on the sand particles, which have a significant role in the formation of biofilms, such as in *C. albicans* biofilms (Alim et al. 2018). Hence, the results depicted in Figs. 10a and 10b demonstrate biofilm formation with the secreted molecules, indicating their potential source of bio-cementation in burrow soil. Another main component of fungal and bacterial EPS are proteins. For instance, glycoproteins, an important SYPRO stained extracellular protein present in fungal EPS, play a key role in nutrient storage and decomposition of soil organic matter (Patel and Gerson 1974; Rajendran et al. 2013; Singh and Das 2020). Extracellular proteins in the burrow sand stained with SYPRO (Bidossi et al. 2020) are shown in Fig. 10c.

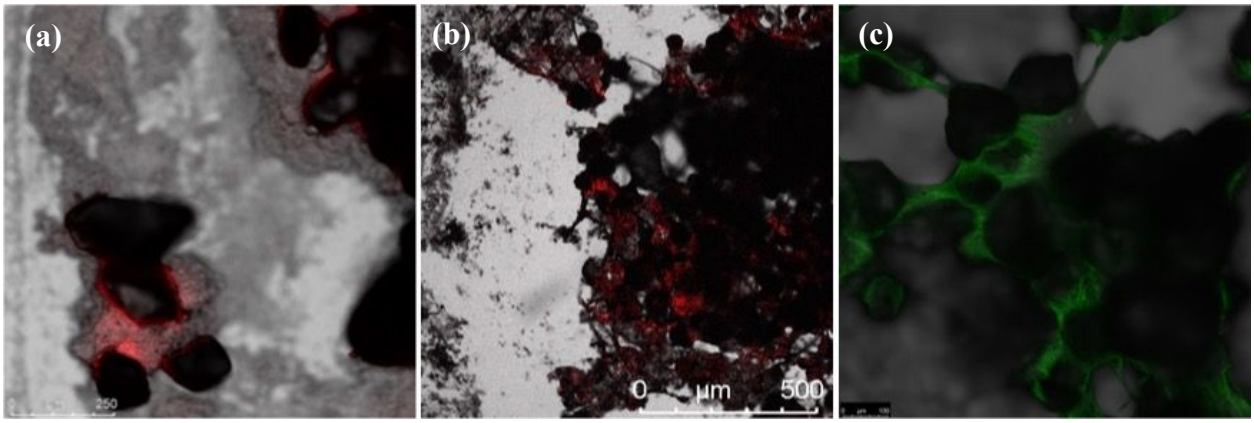

Fig. 10. Confocal microscope images of stained burrow sand samples. Colored region of the images indicated presence of stain specific components. Burrow sand enriched with MEA samples stained with (a) DAPI stain, (b) Nile Blue A stain, (c) SYPRO Ruby biofilm matrix stain.

As demonstrated in the CLSM and SEM images, microbial communities in the burrow sand are capable of secreting EPS, which boosts the formation of biofilm matrix. Therefore, the expected origin of attractive interparticle stresses in burrow soil is the aggregation of biofilm cells and EPS, along with their interconnection with individual sand particles via filamentous structures such as hyphae and mycelium.

4. Practical Implications

The use of bacterial biofilms and fungal mycelium (formation of multiple hyphae) for soil improvement is one of the most recent directions in the field of bio-mediated geotechnics to find cost-effective and environmentally-friendly alternatives to the traditional techniques (Islam et al. 2017; DeJong and Kavazanjian 2019). The majority of the research efforts in this direction have focused on hydraulic modification using microbial biofilms and fungal mycelium and have shown a hydraulic conductivity reduction of up to two orders of magnitude (Ta et al. 2017; Treebupachatsakul and Kamchoom 2021; Kim and Kwon 2022; Salifu et al. 2022; Park et al. 2023). Fewer studies have focused on mechanical modification. Microbial biofilms were shown to increase unconfined compressive strength of sand up to 620 kPa with 25% of mixing concentration by dry mass (Shariq et al. 2021), increased cohesion of sand up to 16 kPa with the mixing percentage of 0.25 by dry mass (Ghatak et al. 2013), or increase shear strength up to 30% (Al-Awad 2018). Fungal mycelium was shown to increase unconfined compressive strength of sand up to 100 kPa with 5 percent fungi inoculum by mass cured 4 days (Lim et al. 2023) and provide erosion resistance (El Mountassir et al. 2021; Zhang et al. 2023). Pure and single species of bacteria or fungi were used in most of these studies and the microorganisms were inoculated for varying durations to promote growth and formation of a mycelium network. Our study used native sand from the kangaroo rat burrows, which showed light cementation in the field. The cementation bonds, and therefore any network structure was broken during sampling and recompaction for laboratory testing. The 17 kPa of attractive stress was obtained in the laboratory by just activating the native microbial and fungal biofilms with the addition of water, without any inoculation (Figure 8). The concentration of fungal and microbial biofilms was less than or approximately equal to 1% by dry mass, based on LOI results (Table 1). The 17 kPa attractive stress obtained without

inoculation, with only 1% of biofilm concentration shows the potential of native microorganisms from kangaroo rat burrows to be used as cementing agents for soil improvement.

5. Conclusions

The stability of kangaroo rat burrows at a site in the Sonoran Desert was evaluated through field and laboratory testing. This study presents a possible mechanism stabilizing kangaroo rat burrows in loose desert sand, which may lead to new sustainable new biocementation agents that can be used in ground improvement applications. The following conclusions are based on test results and analysis:

- Dynamic cone penetration tests in the field showed the presence of a layered burrow structure in the DPI range between 150 and 840 mm/blow. A range of burrow diameters (from 83 cm to 15 cm) were detected in the field especially where the soil profile consisted of loose sand (D_r < 25%).
- The stability of the burrows against collapse was determined using an upper limit equilibrium analysis that considers the resultant interparticle attractive stress as the parameter that provides the burrow stability. The theoretical analysis showed that a minimum of 2.0 kPa attractive stress (for the smallest diameter burrow, if the in-situ packing is SC) and a maximum of 32.1 kPa attractive stress (for the largest diameter burrow, if the in-situ packing is TH) are required to prevent the collapse of the burrows. This indicated that for dry sand, cementation needed to provide 2 to 32 kPa stress to burrow sand, depending on the burrow diameter and in-situ packing.
- Laboratory tests showed that the burrow sand has cementation that for 0.46 void ratio provided 17 kPa attractive stress, which was reactivated only by the addition of water and at less than 1% concentration of organic substances.

- Microscopy imaging and specific staining was used to understand the source of the cementation. SEM images of enriched media samples and stained samples imaged with CLSM showed evidence of fungal growth and microbial biofilms, indicating that the source of the high attractive stress in burrow sand is bio-cementation.
- The high attractive stress due to cementation in the burrow sand makes the fungal and microbial bio-cementation agents in the burrow ceilings potential cementing agents for other geotechnical engineering applications.

Statements and Declarations

The authors have no competing interests to declare that are relevant to the content of this article. The datasets generated during and/or analyzed during the current study are available from the corresponding author on reasonable request.

Acknowledgements

This material is based upon work supported by the National Science Foundation (NSF) under Grant CMMI 2422574. Any opinions, findings, and conclusions or recommendations expressed in this material are those of the authors and do not necessarily reflect the views of NSF. The authors would like to thank Aisha Khamsaysoury for her help with the field work; Jeremy Pennell provided permission to access the Barry M. Goldwater Range West; NHERI RAPID Center for providing the DCP; Analytical Instrumentation Facility (AIF) at North Carolina State University, which is supported by the State of North Carolina and the National Science Foundation (award number ECCS-2025064), Franceschi Microscopy and Imaging Center of Washington State University and Valerie Lynch-Holm for the SEM images.

Permission

No animals were harmed during the procedures of these experiments. All experiments were

conducted in accordance with CSU Sacramento IACUC protocol Cayuse-21-22-3 and Arizona Game and Fish Department License SP059599.

References

Akin, I.D. and Likos, W.J., 2017a. Brazilian tensile strength testing of compacted clay. *Geotechnical Testing Journal*, *40*(4), pp.608-617.

Akin, I.D. and Likos, W.J., 2017b. Implications of surface hydration and capillary condensation for strength and stiffness of compacted clay. *Journal of Engineering Mechanics*, *143*(8), p.04017054.

Akin, I.D. and Likos, W.J., 2020. Suction stress of clay over a wide range of saturation. *Geotechnical and Geological Engineering*, *38*, pp.283-296.

Akin, I.D., Tirkes, S. and Collins, C.E., 2024. Geotechnical insights of mammal burrows in loose desert sand. *Acta Geotechnica*, *19*(3), pp.1449-1459.

Al-Awad, K., 2018. *The effect of biological exudates on the mechanical properties of granular soil* (Doctoral dissertation, Cardiff University)

Alim, D., Sircaik, S. and Panwar, S.L., 2018. The significance of lipids to biofilm formation in Candida albicans: an emerging perspective. *Journal of Fungi*, *4*(4), p.140.

Anderson, A.O. and Allred, D.M., 1964. Kangaroo rat burrows at the Nevada Test Site. *The Great Basin Naturalist*, *24*(3/4), pp.93-101.

ASTM. 2010. D854: Standard test methods for specific gravity of soil solids by water pycnometer. *ASTM International,* West Conshohocken, PA

ASTM. 2006. D4254-00: Standard test methods for minimum index density and unit weight of soils and calculation of relative density. *ASTM International,* West Conshohocken, PA

ASTM. 2017. D-18: Standard practice for classification of soils for engineering purposes (unified soil classification system). *ASTM International,* West Conshohocken, PA

ASTM. 2003. D6951-03: Standard Test Method for Use of the Dynamic Cone Penetrometer in Shallow Pavement Applications. *ASTM International*, West Conshohocken, PA

ASTM. 2009. D6913: Standard Test Methods for Particle-Size Distribution (Gradation) of Soils Using Sieve Analysis. *ASTM International,* West Conshohocken, PA (19428-2959).

ASTM. 2017. D1140: Standard Test Method for Standard Test Methods for Determining the Amount of Material Finer than 75-µm (no. 200). *ASTM International,* West Conshohocken, PA

Atkinson, J.H. and Potts, D.M., 1977. Stability of a shallow circular tunnel in cohesionless soil. *Geotechnique*, *27*(2), pp.203-215.

Belnap, J., Büdel, B. and Lange, O. L. (2001) "Biological soil crusts: characteristics and distribution," in Biological soil crusts: structure, function, and management. Springer, pp. 3–30.

Best, T.L., 1972. Mound development by a pioneer population of the banner-tailed kangaroo rat, Dipodomys spectabilis baileyi Goldman, in eastern New Mexico. *American Midland Naturalist*, pp.201-206.

Bidossi, A., Bottagisio, M., Savadori, P. and De Vecchi, E., 2020. Identification and characterization of planktonic biofilm-like aggregates in infected synovial fluids from joint infections. *Frontiers in Microbiology*, *11*, p.1368.

British Tunnelling Society (BTC), 2004. *Tunnel lining design guide*. Thomas Telford.

Burda, H., Šumbera, R. and Begall, S., 2007. Microclimate in burrows of subterranean rodents—revisited. *Subterranean rodents: news from underground*, pp.21-33.

de Carvalho, C.C., 2017. Biofilms: Microbial strategies for surviving UV exposure. *Ultraviolet light in human health, diseases and environment*, pp.233-239.

Cates, M.E., Wittmer, J.P., Bouchaud, J.P. and Claudin, P., 1998. Jamming, force chains, and fragile matter. *Physical review letters*, *81*(9), p.1841.

Chenu, C., 1989. Influence of a fungal polysaccharide, scleroglucan, on clay microstructures. *Soil Biology and Biochemistry*, *21*(2), pp.299-305.

Chou, C.W., Seagren, E.A., Aydilek, A.H. and Lai, M., 2011. Biocalcification of sand through ureolysis. *Journal of Geotechnical and Geoenvironmental Engineering*, *137*(12), pp.1179-1189.

Davis, E.H., Gunn, M.J., Mair, R.J. and Seneviratine, H.N., 1980. The stability of shallow tunnels and underground openings in cohesive material. *Geotechnique*, *30*(4), pp.397-416.

Decho, A.W., 2000. Microbial biofilms in intertidal systems: an overview. *Continental shelf research*, *20*(10-11), pp.1257-1273.

Decho, A.W. and Gutierrez, T., 2017. Microbial extracellular polymeric substances (EPSs) in ocean systems. *Frontiers in microbiology*, *8*, p.922.

DeJong, J.T. and Kavazanjian, E., 2019. Bio-mediated and Bio-inspired Geotechnics. *Geotechnical fundamentals for addressing new world challenges*, pp.193-207.

Drabek, C.M., 1970. *Ethoecology of the round-tailed ground squirrel, Spermophilus tereticaudus*. The University of Arizona.

Embacher, R.A., 2006. Duration of spring thaw recovery for aggregate-surfaced roads. *Transportation research record*, *1967*(1), pp.27-35.

Espinoza, D.N. and Santamarina, J.C., 2010. Ant tunneling—a granular media perspective. *Granular Matter*, *12*, pp.607-616.

Fraaije, B., Atkins, S., Hanley, S., Macdonald, A. and Lucas, J., 2020. The multi-fungicide resistance status of Aspergillus fumigatus populations in arable soils and the wider European environment. *Frontiers in Microbiology*, *11*, p.599233.

Gattuso, H., Besancenot, V., Grandemange, S., Marazzi, M. and Monari, A., 2016. From non-covalent binding to irreversible DNA lesions: nile blue and nile red as photosensitizing agents. *Scientific Reports*, *6*(1), p.28480.

Ghasemi, P. and Montoya, B.M., 2022. Field implementation of microbially induced calcium carbonate precipitation for surface erosion reduction of a coastal plain sandy slope. *Journal of Geotechnical and Geoenvironmental Engineering*, *148*(9), p.04022071.

Ghatak, S., Manna, S., Roy, D., Saha, P. and Roy, S., 2013. Sand stabilization with exo-polymeric substance producing bacteria isolated from a naturally cemented site. *Proceedings of GeoMontréal*.

Glöckner, F.O., Fuchs, B.M. and Amann, R., 1999. Bacterioplankton compositions of lakes and oceans: a first comparison based on fluorescence in situ hybridization. *Applied and environmental microbiology*, *65*(8), pp.3721-3726.

Gomez, M.G., Martinez, B.C., DeJong, J.T., Hunt, C.E., deVlaming, L.A., Major, D.W. and Dworatzek, S.M., 2015. Field-scale bio-cementation tests to improve sands. *Proceedings of the Institution of Civil Engineers-Ground Improvement*, *168*(3), pp.206-216.

Guo, P. and Zhou, S., 2013. Arch in granular materials as a free surface problem. *International Journal for Numerical and Analytical Methods in Geomechanics*, *37*(9), pp.1048-1065.

Harding, M.W., Marques, L.L., Howard, R.J. and Olson, M.E., 2009. Can filamentous fungi form biofilms?. *Trends in microbiology*, *17*(11), pp.475-480.

Hawkins, L.K. and Nicoletto, P.F., 1992. Kangaroo rat burrows structure the spatial organization of ground-dwelling animals in a semiarid grassland. *Journal of Arid Environments*, *23*(2), pp.199-208.

Heaney, P.J. and Post, J.E., 1992. The widespread distribution of a novel silica polymorph in microcrystalline quartz varieties. *Science*, *255*(5043), pp.441-443.

Holden, P.A., 2001. [9] Biofilms in unsaturated environments. *Methods in Enzymology*, *337*, pp.125-143.

Hondros, G., 1959. The evaluation of Poisson's ratio and the modulus of materials of a low tensile resistance by the Brazilian (indirect tensile) test with particular reference to concrete. *Aust. J. Appl. Sci.*, *10*, pp.243-264.

Horneck, D.A., Hart, J.M., Topper, K. and Koepsell, B., 1989. Methods of soil analysis used in the soil testing laboratory at Oregon State University.

Islam, M.R., Tudryn, G., Bucinell, R., Schadler, L. and Picu, R.C., 2017. Morphology and mechanics of fungal mycelium. *Scientific reports*, *7*(1), p.13070.

Israelachvili, J.N., 2011. *Intermolecular and surface forces*. Academic press.

Jaeger, E.C., 1957. *The North American Deserts*. Stanford University Press.

Jones, E.G., 1994. Fungal adhesion. *Mycological Research*, *98*(9), pp.961-981.

Jones, W.T., 1984. Natal philopatry in bannertailed kangaroo rats. *Behavioral Ecology and Sociobiology*, *15*, pp.151-155.

Kay, F.R. and Whitford, W.G., 1978. The burrow environment of the banner-tailed kangaroo rat, Dipodomys spectabilis, in southcentral New Mexico. *American Midland Naturalist*, pp.270-279.

Kim, Y.M. and Kwon, T.H., 2022. Entrapment of clay particles enhances durability of bacterial biofilm-associated bioclogging in sand. *Acta Geotechnica*, pp.1-11.

Kinlaw, A.L., 1999. A review of burrowing by semi-fossorial vertebrates in arid environments. *Journal of Arid Environments*, *41*(2), pp.127-145.

Lewandowski, Z. and Beyenal, H., 2013. *Fundamentals of biofilm research*. CRC press.

Lim, A., Henzi, P. and Arvin, O., 2023. Comparison Of Pleurotus Ostreatus and Rhizopus Oligosporus Fungi For Loose Sand Improvement. *Journal of GeoEngineering*, *18*(1).

Lovegrove, B.G. and Painting, S., 1987. Variations in the foraging behaviour and burrow structures of the Damara molerat Cryptomys damarensis in the Kalahari Gemsbok National Park. *Koedoe*, *30*(1), pp.149-163.

Loza-Correa, M., Ayala, J.A., Perelman, I., Hubbard, K., Kalab, M., Yi, Q.L., Taha, M., de Pedro, M.A. and Ramirez-Arcos, S., 2019. The peptidoglycan and biofilm matrix of Staphylococcus epidermidis undergo structural changes when exposed to human platelets. *PLoS One*, *14*(1), p.e0211132.

Lu, N. and Likos, W.J., 2006. Suction stress characteristic curve for unsaturated soil. *Journal of geotechnical and geoenvironmental engineering*, *132*(2), pp.131-142.

Mataix-Solera, J., Cerdà, A., Arcenegui, V., Jordán, A. and Zavala, L.M., 2011. Fire effects on soil aggregation: a review. *Earth-Science Reviews*, *109*(1-2), pp.44-60.

Mohammadi, S.D., Nikoudel, M.R., Rahimi, H. and Khamehchiyan, M., 2008. Application of the Dynamic Cone Penetrometer (DCP) for determination of the engineering parameters of sandy soils. *Engineering Geology*, *101*(3-4), pp.195-203.

El Mountassir, G., Schellenger, A., Salifu, E. and Lunn, R.J., 2021. Engineering fungal networks for ground improvement.

NOAA, National Centers for Environmental Information, N. O. and A. A. data (2022) *YUMA MCAS, AZ US (USW00003145), Past Weather*. Available at: https://www.ncei.noaa.gov/access/past-weather/yuma, az.

Ostle, A.G. and Holt, J.G., 1982. Nile blue A as a fluorescent stain for poly-beta-hydroxybutyrate. *Applied and environmental microbiology*, *44*(1), pp.238-241.

Park, J., Kim, M., Shin, B., Kang, M., Yang, J., Lee, T.K. and Park, W., 2021. A novel decoy strategy for polymyxin resistance in Acinetobacter baumannii. *Elife*, *10*, p.e66988.

Park, J.S., Lin, H., Moe, W.M. and Salifu, E., 2023. Hydraulic properties of sands treated with fungal mycelium of Trichoderma virens. *Journal of Geotechnical and Geoenvironmental Engineering*, *149*(11), p.04023093.

Patel, J.J. and Gerson, T., 1974. Formation and utilisation of carbon reserves by Rhizobium. *Archives of microbiology*, *101*, pp.211-220.

Peberdy, J.F. and Peberdy, J.F., 1980. Vegetative Growth of Filamentous Fungi. *Developmental Microbiology*, pp.44-68.

Pietrasiak, N., Regus, J.U., Johansen, J.R., Lam, D., Sachs, J.L. and Santiago, L.S., 2013. Biological soil crust community types differ in key ecological functions. *Soil Biology and Biochemistry*, *65*, pp.168-171.

Powers, M.C., 1953. A new roundness scale for sedimentary particles. *Journal of Sedimentary Research*, *23*(2), pp.117-119.

Rajendran, R., Williams, C., Lappin, D.F., Millington, O., Martins, M. and Ramage, G., 2013. Extracellular DNA release acts as an antifungal resistance mechanism in mature Aspergillus fumigatus biofilms. *Eukaryotic cell*, *12*(3), pp.420-429.

Reichman, O.J., Wicklow, D.T. and Rebar, C., 1985. Ecological and mycological characteristics of caches in the mounds of Dipodomys spectabilis. *Journal of Mammalogy*, *66*(4), pp.643-651.

Rodriguez-Navarro, C., Rodriguez-Gallego, M., Ben Chekroun, K. and Gonzalez-Muñoz, M.T., 2003. Conservation of ornamental stone by Myxococcus xanthus-induced carbonate biomineralization. *Applied and environmental microbiology*, *69*(4), pp.2182-2193.

Salifu, E., El Mountassir, G., Minto, J.M. and Tarantino, A., 2022. Hydraulic behaviour of fungal treated sand. *Geomechanics for Energy and the Environment*, *30*, p.100258.

Santamarina, J.C. and Fam, M., 1995. Changes in dielectric permittivity and shear wave velocity during concentration diffusion. *Canadian Geotechnical Journal*, *32*(4), pp.647-659.

Santamarina, J.C., Klein, A. and Fam, M.A., 2001. Soils and waves: Particulate materials behavior, characterization and process monitoring. *Journal of Soils and Sediments*, *1*(2), pp.130-130.

Scalia IV, J., Benson, C.H., Bohnhoff, G.L., Edil, T.B. and Shackelford, C.D., 2014. Long-term hydraulic conductivity of a bentonite-polymer composite permeated with aggressive inorganic solutions. *Journal of Geotechnical and Geoenvironmental Engineering*, *140*(3), p.04013025.

Schofield, A.N., 2006. Interlocking, and peak and design strengths. *Geotechnique*, *56*(5), pp.357-358.

Shariq, A.F., Beyenal, H. and Akin, I.D., 2021. Biofilm addition improves sand strength over a wide range of saturations. *Biofilm*, *3*, p.100050.

Sichilima, A.M., Bennett, N.C., Faulkes, C.G. and Le Comber, S.C., 2008. Evolution of African mole-rat sociality: burrow architecture, rainfall and foraging in colonies of the cooperatively breeding Fukomys mechowii. *Journal of Zoology*, *275*(3), pp.276-282.

Singh, S.P. and Das, R., 2020. Geo-engineering properties of expansive soil treated with xanthan gum biopolymer. *Geomechanics and Geoengineering*, *15*(2), pp.107-122.

Ta, H.X., Muhunthan, B., Ramezanian, S., Abu-Lail, N. and Kwon, T.H., 2017. Effects of bacterial dextran on soil geophysical properties. *Environmental Geotechnics*, *5*(2), pp.114-122.

Takano, Y.H., 2000. Guidelines for the design of shield tunnel lining (ITA WG 2 report). *Tunn. Under. Space Technol.* 15 (3), 303–331.

Tisdall, J.M. and Oades, J.M., 1979. Stabilization of soil aggregates by the root systems of ryegrass. *Soil Research*, *17*(3), pp.429-441.

Tisdall, J.M. and OADES, J.M., 1982. Organic matter and water-stable aggregates in soils. *Journal of soil science*, *33*(2), pp.141-163.

Treebupachatsakul, T. and Kamchoom, V., 2021. Permeability and setting time of bio-mediated soil under various medium concentrations. *Journal of Rock Mechanics and Geotechnical Engineering*, *13*(2), pp.401-409.

Valdes, J.R. and Santamarina, J.C., 2006. Particle clogging in radial flow: Microscale mechanisms. *Spe Journal*, *11*(02), pp.193-198.

Vorhies, C.T. and Taylor, W.P., 2022. *Life history of the kangaroo rat*. DigiCat.

Wingender, J., Neu, T.R. and Flemming, H.C., 1999. *What are bacterial extracellular polymeric substances?* (pp. 1-19). Springer Berlin Heidelberg.

Youd, T.L., 1973. Factors controlling maximum and minimum densities of sands. In *Evaluation of relative density and its role in geotechnical projects involving cohesionless soils*. ASTM International.

Zhang, X., Fan, X., Wang, C. and Yu, X., 2023. A novel method to improve the soil erosion resistance with fungi. *Acta Geotechnica*, *18*(5), pp.2827-2845.